Modeling of plasma dynamics in x-ray-confining cavities

J. Massen, G. D. Tsakiris, and R. Sigel
Max-Planck-Institut für Quantenoptik, D-85748 Garching, Federal Republic of Germany
(Received 4 May 1993)

The effect of the plasma expansion from the wall of a laser-heated spherical cavity and its collision at the center of the cavity has been studied using the MULTI hydrocode. The simulations show an enhancement of the circulating x-ray flux due to kinetic-energy conversion into internal energy in the colliding plasma. The results of the simulations have been compared with the experimental observations from triple cavity targets. This comparison provides additional insight into the processes occurring in laser as well as in x-ray-heated cavities.

PACS number(s): 52.50.Jm, 44.40.+a, 47.70.Mc, 52.25.Nr

I. INTRODUCTION

Heating of millimeter-size gold cavities by high-power lasers has been used as a means of creating very intense, isotropic hohlraum radiation in the soft-x-ray range [1–6]. Temperatures of several million degrees kelvins and fluxes of up to 10^{15} W/cm^2 seem to be achievable nowadays [7,8]. The intense thermal radiation created inside a closed geometry target such as a cavity is of interest because it has a number of applications, the most notable of which is the indirect drive inertial confinement fusion (ICF) [9–11]. Furthermore, the closed geometry targets provide the possibility of studying in the laboratory a number of radiation hydrodynamics related topics [12,13].

The principle of cavity heating using a high-power laser is simple. The laser beams are focused through a small entrance hole into the cavity where they irradiate a small part of the inner wall surface. At this directly heated by the laser-beam area, a conversion plasma is produced emitting primary x rays which carry the energy across the whole cavity. The reemission of thermal radiation from the x-ray-heated cavity wall leads finally to the formation of an isotropic radiation field in the soft-x-ray range [14].

The heating of a wall by intense thermal radiation is a classical problem of radiation hydrodynamics [15–17]. Upon irradiating a surface element with intense thermal flux, the radiation diffuses into the high-Z material giving rise to a propagating heat wave. The heat wave thus formed is of the ablative type, i.e., it is followed by expansion of hot plasma into the vacuum. In closed-geometry targets (e.g., spherical or cylindrical cavities), the plasma expansion has the consequence that, after some time, the space inside the cavity is completely filled with plasma. If this plasma filling time is considerably longer than the laser-pulse duration, then its effect can be neglected and the cavity can be considered as empty. This was the tacit assumption employed in the interpretation of the experimental results from previous experiments [1–8]. However, there are two important reasons why one should study in detail the plasma dynamics in a cavity. The first reason is simply the fact that, for a given laser energy and pulse duration, the smaller the cavity, the higher the temperature that can be achieved. The characteristic dimension of a cavity therefore should be chosen as a compromise between keeping the inner cavity space plasma free and heating the cavity at the maximum possible temperature. To establish the correct criteria by means of which a delimiting radius can be calculated, it is necessary to study the primary (laser) and secondary (x-ray) plasma expansion inside the cavity.

The second reason is in the context of the indirect drive approach to ICF. In this case the cavity contains the pellet with the fuel and the plasma dynamics has important consequences for the energy balance and ultimately the pellet performance in the cavity [18]. Stagnation of the plasma blowoff can result in refraction of the incident laser beams. It can give rise to additional sources of radiation since the kinetic energy of the expansion is converted back into internal energy. It can provide a bridge to transfer energy to the pellet via electron thermal conduction and can exert hydrodynamic pressure.

In order to elucidate the physical process occurring inside a laser-heated cavity, we have performed numerical simulations using the hydrocode MULTI [19]. This is a one-dimensional, fully implicit code that solves Lagrangian hydrodynamics together with multigroup radiation diffusion. Although MULTI is only a one-dimensional Lagrangian code it is possible to calculate three-dimensional objects with spherical symmetry and to use spatially fixed Eulerian coordinates for incorporating the appropriate boundary conditions. These special features make it possible to take into account the real size of a cylindrical or a spherical cavity. In performing the simulations, attention has been focused on the effects of plasma filling, collision, and stagnation in spherical cavities and their consequences to the establishment and confinement of the radiation field inside the cavity. The organization of this paper is as follows: The numerical model employed is described in detail in Sec. II. The results of the simulations are presented in Sec. III while in Sec. IV, a comparison is made with some earlier experimental results. The main conclusions are summarized in Sec. V.

II. THE SIMULATION MODEL

It has been shown [16] that in the case of a wall irradiated by intense thermal radiation, the space- and time-dependent planar hydrodynamics equations with radiative heat conduction admit a self-similar solution, which leads to a scaling law for the wall temperature as a function of time t and net radiant flux S_w that supplies energy to the ablative heat wave (AHW) propagating in the cold material, namely

$$T_r(t)=c't^{\alpha'}S_w^{\beta'} . \tag{1}$$

The constant c' and the exponents α' and β' are related to the physical properties of the wall material. One of the most important material properties is the Rosseland mean free path for the radiation which determines the coefficient for radiative heat conduction. The Rosseland opacity for several materials and its functional dependence on temperature and density has been calculated in the average ion approximation [20] and the results have been used to determine the constant and the exponents in Eq. (1).

Using Stefan-Boltzmann's relation, one obtains the following expression for the reemitted flux:

$$S_r(t)=\sigma T_r^4(t)=ct^{\alpha}S_w^{\beta} , \tag{2}$$

where $c=\sigma c'^4$, $\alpha=4\alpha'$, $\beta=4\beta'$, and σ is the Stefan-Boltzmann constant. For the material employed most commonly in experiments, gold, one obtains the following numerical values using the corresponding opacity scaling on temperature and density [21]:

$$T_r=262.2\tilde{t}^{2/13}\tilde{S}_w^{4/13} \text{ eV} , \tag{3}$$

$$\tilde{S}_r=4.87\tilde{t}^{8/13}\tilde{S}_w^{16/13} . \tag{4}$$

Here the reemitted $\tilde{S}_r$ and wall $\tilde{S}_w$ flux are in units of 10^{14} W/cm^2 and time $\tilde{t}$ in units of 10^{-9} s. The opacity data from Ref. [20] have been used to obtain the numerical values.

A simple analytical estimate for the temperature T_r inside a heated cavity possessing openings can be obtained from the expression [21]

$$S_r=ct^{\alpha}(S_s-n^{-1}S_r)^{\beta} . \tag{5}$$

It is based on the scaling law in Eq. (2) and the flux balance at the surface of the wall which gives the wall flux S_w in terms of the source flux S_s and the fractional hole area n^{-1}, i.e., $S_w=S_s-n^{-1}S_r$. The fractional hole area n^{-1} is defined as the ratio between the open area to the total area of the cavity. By solving the implicit relation in Eq. (5) for S_r, one obtains an estimate of the wall temperature for an externally delivered heat flux S_s and for a heating period t.

Unfortunately, the assumption of plane geometry underlying the analytical solution (AHW) restricts the application of the formula in Eq. (5) to ideal cavities of infinite size or at least to cavities with a diameter which is large compared with the typical extent of the plasma at the end of the heating period. As was already pointed out, in order to reach high intensities and temperatures, one is forced to use cavities as small as possible. Hence it cannot be excluded that during the heating period, the cavities are quickly filled with plasma. The plasma filling and stagnation is expected to have a crucial influence on the temperature measurement, thus making a more detailed investigation necessary. For that purpose, the only applicable model in which the finite size of the cavity is taken into account would be one based on the hydrocode MULTI. The hydrocode, apart from being a numerical model, has a number of advantages over the analytical solution and provides a more realistic and comprehensive calculation of the effects due to plasma expansion. These advantages are enumerated in Table I.

The hydrocode and the analytical solution (AHW) are two alternative methods to estimate the wall temperature of a "large" cavity. The analytical solution which is valid for some well-defined boundary conditions can serve as a test case for the simulation model. A particularly well-suited case for this purpose is the planar geometry with radiation losses. Alternatively, the hydrocode can be used to check the validity of the restrictive assumptions involved in the analytical model (e.g., complete thermodynamic equilibrium; see also Table I). To illustrate this, we have made a comparison between the hydrocode and the analytical model for some special cases.

The simulations were carried out with the arrangement shown in Fig. 1. The cavity is assumed to possess spherical symmetry, therefore the interior wall is uniformly heated by laser as well as by thermal x-ray radiation. A small hard sphere ($r_{\text{hard sphere}}\approx r_{\text{cavity}}/10$) in the center of the cavity reflecting the radiation serves to avoid numerical difficulties. It was found that all variables of interest, e.g., cavity temperature, total emission, emission due to collision, etc, do not depend sensitively on the radius of the hard sphere. This was established by varying the

TABLE I. Comparison of the assumptions involved in the analytical solution and hydrocode.

Analytical model (AHW)	Hydrocode (MULTI)
Complete thermodynamic equilibrium between radiation and matter (conduction approximation)	Finite optical thickness, spectral resolution (diffusion approximation)
Idealized source (thermal x rays)	Conversion of laser light to x rays
Planar geometry only	Three geometries (1D)
Infinitely large cavity	Finite-size cavity
Constant source flux	Arbitrary pulse shape

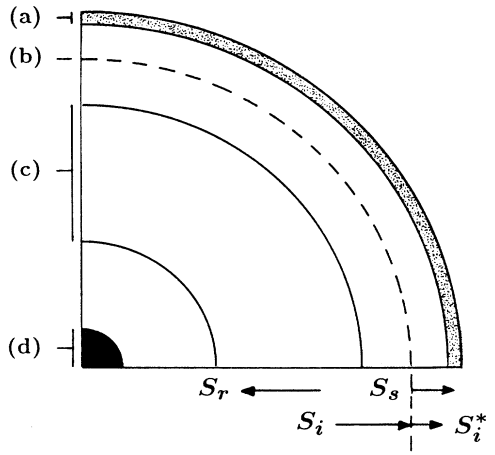

FIG. 1. Schematic showing the division of the cavity interior into different regions for the 1D simulations based on the MULTI hydrocode. Represented regions are the (a) cavity wall (~ 10 μm) and (b) interface where the source flux S_s (laser or x rays) is coupled into the material. At the same interface the incident flux S_i is reduced to S_i^* to simulate losses due to cavity openings: (c) area where the reemitted flux S_r is recorded and stored for subsequent calculations (for example, see inset in Fig. 3) and (d) small hard sphere with radius $\sim r_{\text{cavity}}/10$ introduced to avoid numerical difficulties.

hard-sphere radius by $\pm 50\%$. The source flux S_s (laser or thermal x rays) is coupled to the material at a spatially fixed interface near the cavity wall. To simulate the cavity with losses, the incident flux from all other wall elements of the cavity S_i is reduced by a given factor resulting in the flux $S_i^* = (1 - n^{-1}) S_i$. The probing of the cavity confined radiation field is performed by measuring the reemitted flux S_r at the space between wall and cavity center (see Fig. 1).

It must be mentioned here that some important modifications had to be introduced to the original version [19] of the basically Lagrangian code MULTI in order to be able to follow the expansion of the wall plasma and its implosion at the center of the cavity. These changes mainly affect the input and the output quantities and not the numerical procedure which is employed to solve the hydrodynamical equation with radiation transfer. For example, in these simulations the laser energy is coupled to the plasma at a fixed point in space (Euler coordinate) and not to a fixed mass element (Lagrange coordinate). This was necessary because, in the case of a Lagrangian code, a mass element moves with expanding plasma towards the center of the cavity. The material that is then accumulated there is laser heated and it expands again before the real collision and compression sets in, thus preventing the collision from fully developing. This applies to radiation losses as well, which can be accurately defined only at an interface of well-known spatial extent. Furthermore, the temperature should be observed at a point which is clearly identifiable within the spatial temperature distribution and at an area where the radiation field is approximately constant in space away from sources and sinks.

For studying the effect of the expanding plasma, it is convenient to introduce a magnification factor M. In the simulations, the cavity radius is multiplied by M while the laser energy by M^2. This permits the variation of the cavity size while the irradiation intensity remains constant. A value of $M = 1$ corresponds to the real cavity size in which plasma collision takes place. On the other hand, for $M = 10-100$, the plasma expansion represents a very small fraction of the cavity radius and thus the planar geometry can be simulated. The latter case can be directly compared with the predictions of the analytical model. As discussed in Sec. III, the difference in the reemitted flux S_r between the two cases ($M = 1$ and 10) would be due exclusively to plasma stagnation and collision at the center of the real size cavity.

Figures 2 and 3 depict the degree of agreement between analytical solution and hydrocode in two different situations. In this case, in order to ensure that the hydrocode correctly simulates the planar geometry assumed in the analytical model, we have used a magnification factor of $M = 100$. The purpose of the first comparison depicted in Fig. 2 is to check the assumption of complete thermodynamic equilibrium involved in the analytical solution. For that purpose, we have compared the temporal evolution of the reemitted flux inside a cavity heated by a constant in time x-ray source. We have considered only the case of closed cavities ($n^{-1} = 0$) because for partially or completely open geometry, the reemitted flux converges very quickly towards a limit which is independent of the scaling law for wall heating and therefore not interesting for this comparison. This limit can be obtained by setting the source energy equal to the energy losses through the holes [21]. The comparison in Fig. 2 shows good agreement in absolute values as well as in the scaling of the reemitted flux S_r after a certain early stage. The discrepancy between hydrocode and analytical solution during the early stages suggests that it takes some time and energy to establish an optically thick self-similar ablative heat wave in complete local thermodynamical equilibrium [22]. The late time deviation for higher source

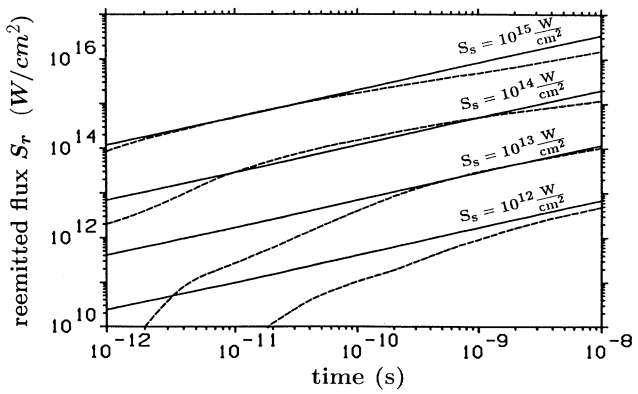

FIG. 2. Temporal evolution of the reemitted flux S_r from the wall of a closed cavity as predicted by the simulations (dashed line) and the analytical model (AHW) (solid line) for the indicated constant in time source flux values.

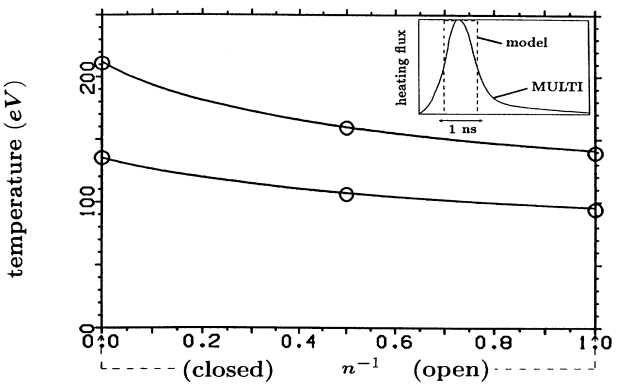

FIG. 3. Variation of the temperature enhancement in cavities possessing different degrees of fractional area n^{-1}. The predictions from the analytical model (AHW) are represented by the solid lines, while from the simulations and for $n^{-1}=0$ (completely closed cavity), $n^{-1}=0.5$ (cavity with 50% of its surface removed), and for $n^{-1}=1$ (planar target) by open circles. In the simulations a realistic heating pulse is employed, which was taken from a previous conversion calculation (see inset). On the contrary, the analytical model uses an equivalent flat top pulse with an irradiation intensity of 1.3×10^{13} (lower curve) and 5.5×10^{13} W/cm^2 (upper curve) and a pulse duration of 0.8 ns.

fluxes can be attributed to similar reasons. In the analytical model the spectral composition of the generated radiation within the layer is not taken into account. Prolonged heating periods and higher source fluxes result in higher temperatures [compare Eq. (1)]. This gives rise to radiation containing a non-negligible amount of gold M-shell line radiation ($h\nu\approx3$ keV) for which the layer is not optically thick [23]. As a result, there is a certain amount of degradation in the reemission.

The second situation we have compared is that of a cavity with variable losses (cavity openings). This was done to establish whether the hydrocode and the analytical model are in agreement in predicting the reduction of the reemitted flux S_r due to losses through cavity openings. This is depicted in Fig. 3 where the cavity temperature as a function of the fractional hole area is given. In order to make the simulations more realistic and closer to the experiments, we have this time used a heating pulse (see inset in Fig. 3). It was taken from a separate run of the code which only served to calculate the conversion of the laser energy into x-ray radiation and numerically store it. By changing the pulse shape of the source radiation in relation to the analytical model, we do not observe a significant effect on the final temperature reached in the simulations. As usual the analytical model assumes a flat top source pulse with the same energy content. The results of the code and the analytical solution are presented in Fig. 3. As can be seen the simulations reproduce the dependence of the reemitted flux on the fractional hole area and in particular the temperature enhancement in closed cavities very well. The observation of this good agreement in both situations justifies our confidence in the hydrocode results and its usage for the investigation of the plasma filling in small cavities.

III. PLASMA DYNAMICS IN A FINITE-SIZE CAVITY

To illustrate the capabilities of the numerical model based on the hydrocode MULTI, we present here an example of a calculation for a completely closed cavity (no losses) having a diameter of 1 mm. The interior wall of the cavity was uniformly irradiated according to the scheme illustrated in Fig. 1 with ~3 kJ of energy of $\lambda=0.35$ μm (3ω) Nd-glass laser light having a pulse duration of $\tau_L=0.9$ ns. These data are relevant to the conditions prevailing in the laser-heated cavities in previously performed experiments [6,8,13] (more detailed information is given in Sec. IV).

The results of the simulations are presented in Fig. 4 by means of two-dimensional isocontour plots. In these plots the different regimes can be easily distinguished. The evolution of the plasma density in the cavity interior is shown in Fig. 4(a) whereas in Fig. 4(b) the evolution of the divergence of the x-ray flux ($\nabla\cdot\mathbf{S}$) for each radial position is given. This quantity provides additional information abut the energy redistribution inside the cavity since $\nabla\cdot\mathbf{S}>0$ means production of radiation whereas $\nabla\cdot\mathbf{S}<0$ means absorption [hatched areas in Fig. 4(b)]. According to our model in Fig. 1, the cavity wall of ~10 μm thickness is located ~0.5 mm from the cavity center. The center itself (10% of the cavity radius) is not included in the plot. It is the volume of the small hard sphere (no loss of energy or momentum) which, as already explained, is introduced for technical reasons, i.e., to smooth out the singularity at the cavity center. In reality, this artificial hard sphere can be said to represent the radius at which the density of the plasma is so high that the ions acquire a very short mean free path and they cannot penetrate any further.

The plasma expansion and the subsequent radiation production can be now followed by simultaneous study of the two plots in Fig. 4. At the beginning of the laser pulse, the inner cavity space remains empty [Fig. 4(a) while according to the plot in Fig. 4(b), a region of intense x-ray production near the inner side of the wall develops. Here the laser radiation is absorbed and converted into thermal x rays. The hatched area to the right describes the absorption of thermal x rays by the cold cavity wall. Starting from this location, the laser (primary) plasma expands to the left into the void of the cavity while the wall is accelerated outwards. As can be seen most of the cavity volume is quickly filled up with expanding low-density plasma and with x-ray radiation of very uniform intensity ($\nabla\cdot\mathbf{S}\approx0$). Due to the high temperature of the laser heated plasma, a very high expansion velocity is reached. Within 1 ns the radial distance of 500 μm is covered and the plasma front arrives at the center of the 1-mm cavity. As a consequence of the collision the density rises strongly up to 1/10 solid density. The kinetic energy of the laser plasma is converted into thermal energy and the temperature reaches values of several keV. The resulting combination of density temperature at the central region results in significant radiation production ($\nabla\cdot\mathbf{S}>0$) seen in Fig. 4(b) at ~1 ns after the beginning of the laser pulse ($t=0$). It persists for ~1 ns and is localized in the region between 0.5 and 0.15 mm. This radiation constitutes an additional contribu-

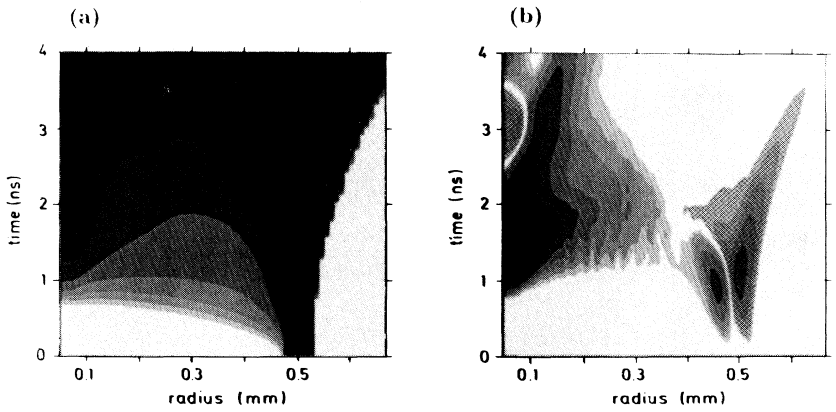

FIG. 4. Temporal and spatial evolution of (a) the density and (b) the divergence of the radiation flux in the interior of a lossless 1-mm cavity uniformly irradiated with $\sim 10^{14}$ W/cm^2 of $\lambda = 0.35$-μm (3ω)Nd-glass laser light having a pulse duration of $\tau_L = 0.9$ ns. In the contour plots, the values are normalized to the maximum, the steps are logarithmic, and comprise four decades in case (a) and two decades in case (b). Opposed to emission, absorption is characterized by the hatched area.

tion to the heating of the cavity wall. For the 1-mm cavity we observe a partial temporal overlap of the spatially separated primary source flux and the collisionally produced x rays which leads to a remarkable rise in cavity temperature.

In the experiments, the spherical symmetry assumed in our model calculations is not achieved. But reheating of the cavity by kinetic to thermal energy conversion after stagnation of the expanding plasma takes place in any case. To obtain a quantitative estimate of the reheating contribution from the collision, we have carried out calculations with different size cavities heated with the same irradiation intensity (see Sec. II). Comparing the case $M = 10$ (no collision) with the case $M = 1$ (with collision), we found a maximum radiation flux in the real 1-mm cavity ($M = 1$) where collision takes place that is higher by a factor of 1.6 than that without collision ($M = 10$).

IV. DISCUSSION AND COMPARISON WITH EXPERIMENTS

The motivation for the simulations presented in this paper is the in depth interpretation of the experimental results obtained with the triple cavity targets shown in Fig. 5. They consist of a central-laser-heated converter cavity which irradiates through connecting openings two satellite cavities with thermal x rays. The difference between the two satellite cavities is that the upper one has a minimal amount of radiation losses due to small openings (diagnostic holes only) while the lower one is made to maximize them [see Fig. 5(b)]. This way the closed and open geometry is realized. Two different size cavities were used, those with 1 mm diameter (all three cavities) and those with 2 mm. The most important results from these experiments have been already reported [6,8] and a more detailed account of the experimental setup, data analysis, and interpretation can be found in Ref. [24]. As is described in Ref. [6], we were able to directly demonstrate the occurrence of radiation confinement by comparing the radiation temperature of a confining (closed) cavity to that of a nonconfining (open) cavity.

We return to these experimental results with the intention to use the numerical model based on the hydrocode MULTI to try to understand the more subtle features and simultaneously to assess the role of the plasma stagnation and collision in these targets. An extension of the theoretical results summarized in Sec. II for a single cavity to the more general case of two interacting (coupled) cavities has already been worked out [6,24]. This analytical model, appropriate for the new kind of targets consisting of three coupled cavities reaching different temperatures, is based on the AHW and describes the radiation confinement as well as the energy exchange between the cavities through the connecting openings.

However, as we pointed out in Sec. II, the description of the cavity heating by the analytical solution is not

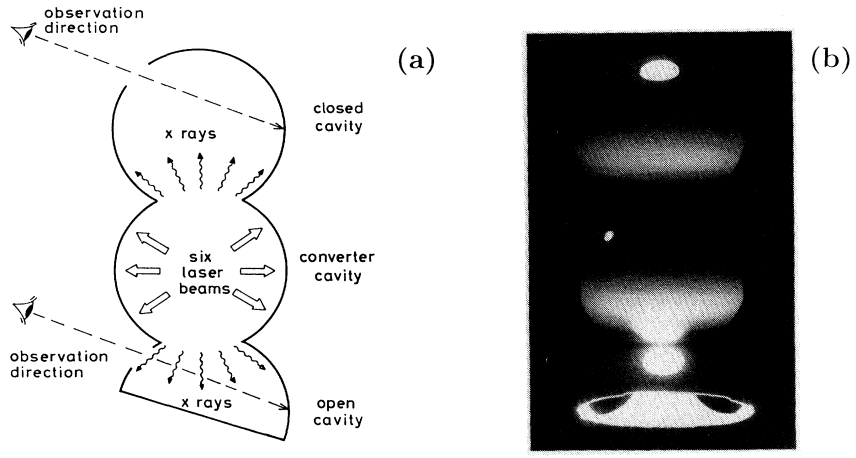

FIG. 5. (a) Schematic diagram showing the sequence of heating and the method of observation in the triple cavity targets. (b) Scanning electron microscope photograph of the real target.

complete. One important process, namely the plasma flow and stagnation, is not included in the analytical solution based on the AHW. We saw that for "small" size cavities reheating by plasma collision is important. Focusing our attention on the comparison between the model calculations and the experimental results in order to come to an interpretation, it is reasonable to distinguish between the two cavity dimensions. The cavities with 1 mm diameter suffer plasma stagnation and collision and therefore belong to the category of "small" cavities while the cavities with 2 mm diameter are closer to the ideal case of "large" cavities.

The simulation of the triple cavity targets using the model described in Sec. II takes place in two steps. In the first step the converter (middle) cavity is simulated by irradiating the interior surface of the cavity with an average energy density $\mathcal{E}_L^{\text{av}}=E_L/\pi D^2$ where E_L is the laser energy and D the cavity diameter. Here the assumption is made that the laser energy is uniformly distributed over the inner cavity surface (necessary condition since MULTI assumes spherical symmetry). In the experiment, the laser spots are uniformly distributed over an annular region of the cavity wall [see Fig. 5(a)]. This arrangement leads to a concentric flow of laser plasma towards the center of the cavity thus rendering the assumption of uniform illumination as reasonable. The laser pulse shape is approximated by a $\cos^2 t$ form having a duration of $\tau_L=0.9$ ns. The cavity losses are calculated based on the total open area (including the connecting openings) of the converter cavity. From this run the temporal evolution of the converter cavity temperature is obtained. The corresponding flux, appropriately diluted by the coupling factor resulting from the connecting openings, is numerically stored and used in the second step to irradiate the two satellite cavities. This follows in two separate runs where the appropriate losses for the closed and open cavity are introduced.

The main results of these simulations and a comparison with the experimental results and analytical solution predictions [6,24] are pictorially presented in the diagram of Fig. 6. One observes, within experimental accuracy, good agreement between experimental results, simulations, and the analytical model for both cavity sizes. However, the main effect we are after is the plasma expansion and collision at the center of the cavity and its influence on the final temperature reached in each individual cavity. This effect is also depicted in Fig. 6 where the results without collision ($M=10$) are represented by full circles that have to be moved where the full squares are when collision is taken into account ($M=1$). As can be seen, the 2-mm cavities do not show any temperature enhancement due to plasma stagnation and collision. In contrast, the 1-mm-cavity results indicate that there is a temporal overlap between the laser pulse and plasma collision, leading to an evident enhancement of the temperature at first in the converter cavity and subsequently in the satellite cavities. It is to be noted here that, as expected, the analytical model results for the 1-mm cavities are in good agreement with the $M=10$ simulations while the experimental results confirm the existence of the plasma collision, i.e., agree well with the $M=1$ simulations.

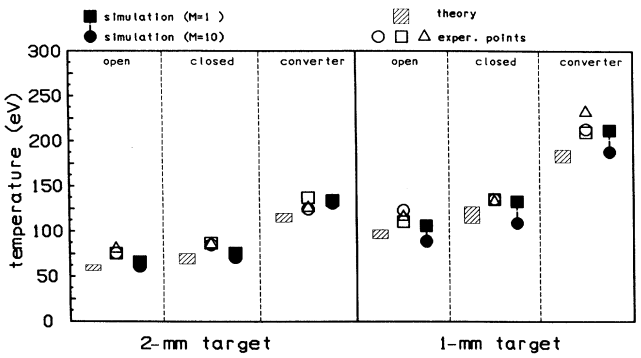

FIG. 6. Comparison of radiation temperature in experiment, simulations, and analytical model for each individual cavity of the 2- and 1-mm triple cavity targets (see also Fig. 5). The simulation results are given by the full circles and full squares. The distance between them represents the effect of the plasma collision in each cavity. The analytical calculations (theory), given by the hatched rectangles, take into account the uncertainty in the heating period of the converter cavity due to laser light reflection as a consequence of plasma filling. The top of the rectangle corresponds to 0.9 ns, i.e., the laser-pulse duration, the bottom to 0.4 ns, the shortest measured x-ray pulse duration.

Another signature of the plasma collision in the cavity interior is to be found in the time history of the x-ray signal emanating from the diagnostic holes. From our simulations we expect that there is no possibility to separate the collision peak from the laser heating in the 1-mm cavity. However, in the 2-mm cavity the plasma requires more time to reach the center and to collide not only because of the larger distance that it has to travel but also due to lower values of irradiation fluxes. So, in this case, we expect a second clearly separated peak of x-ray emission due to collisional reheating in the converter cavity. Figure 7 illustrates the experimental results and the simulation. The temporal evolution of the radiation temperature measured in the satellite cavities shows the same behavior as in the simulation, i.e., two peaks corresponding to the laser heating and the collisional reheating. The exact location of the collisional peak with respect to the laser peak is not accurately reproduced by our simulations. This is due to the fact that the local irradiation intensity in the simulation is lower than in the experiments since the same energy is distributed over the whole inner-cavity surface and not on an annulus as in the experiment (see also Sec. III). This was confirmed by separate code runs where the average irradiation intensity was varied resulting in a movement of the two peaks relative to each other.

It is seen that the second peak in the converter cavity signal is missing from the experimental data. In order to avoid overexposure of the detector [6], the diagnostic hole in the converter cavity was only 100 μm in diameter, considerably smaller than the holes in the satellite cavities (400 μm), where the radiation temperature was lower. The abrupt reduction of the x-ray signal from the converter cavity is thus attributed to hole closure by expanding wall plasma. Estimations based on a simple model by

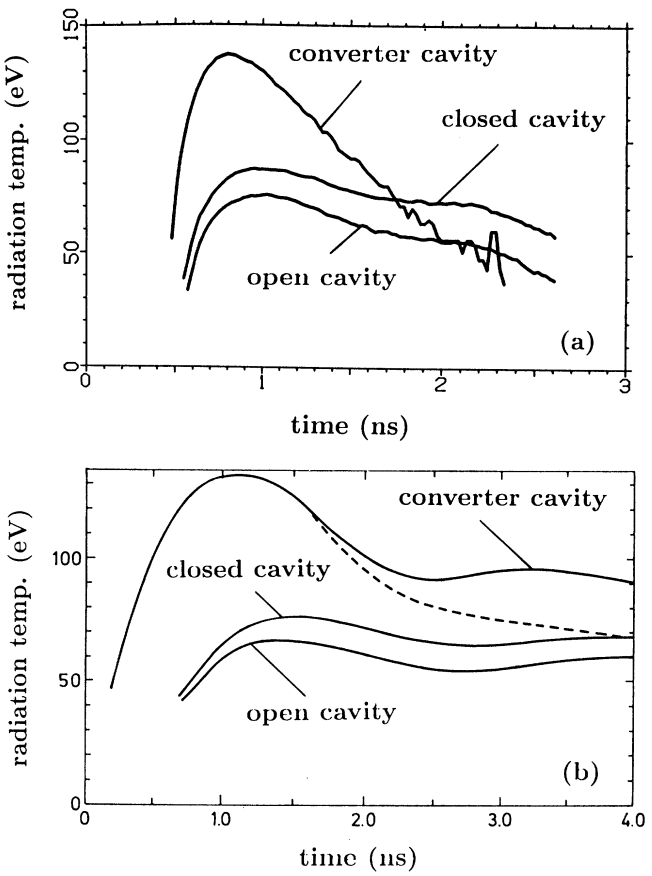

FIG. 7. Temporal evolution of the radiation temperature in the partial cavities of a 2-mm triple cavity target. Comparison of the experimental data (a) with the MULTI simulations (b). The dashed line represents the modification to the observed radiation temperature resulting from hole closure as it is simulated with the hydrocode MULTI.

Harrach and Gee [25] have shown that the enclosure time for the diagnostic hole in the central cavity is much shorter than the laser-pulse duration. This effect can also be simulated using the model in Sec. II by introducing a spatially fixed point at a distance of 100 μm from the wall inside the cavity, where the radiation temperature is monitored. This distance corresponds to the diameter of the diagnostic hole. When the expanding cold-wall plasma passes by, the observed point is isolated from the hot radiating inner volume of the cavity, as our instruments were isolated by the cold hole plasma. This simulation gives the dashed line in Fig. 7(b), a very quickly falling temperature curve (even falling below the temperature curves of the satellite cavities), such as that observed in the experiment. Because no other cooling mechanism could be found that would initiate the observed rapid temperature fall and because this is observed in the converter cavity only, we conclude that hole closure is indeed responsible for this temporal behavior.

V. SUMMARY

For the study of radiation confinement in the presence of plasma expansion in real size cavities, we have developed a special scenario to simulate effects such as plasma filling and stagnation, and the resulting collision and reheating of the cavity. This scenario is based on the one-dimensional hydrocode MULTI. In addition, other effects such as hole losses in a partially opened cavity and hole closure can also be simulated. In a parameter range in which there exists a validity overlap , very good agreement was observed between the analytical solution for the AHW and the simulation model. For example, for "large" cavities, the two calculations gave practically the same results for the confined radiation field under variation of source flux, pulse duration, pulse shape, and openness of the cavity. A notable exception is an early stage of a few hundred picoseconds, depending on the laser energy, during which full equilibration of radiation and matter has not yet been established and, as a consequence, the radiation intensity is considerably lower than the one predicted analytically.

Extending the application of our simulations to the cases of interest, i.e., real size cavities, we saw the plasma, expanding from the cavity wall colliding in the center, thermalizing its kinetic energy, and reheating the cavity. In the center densities of nearly $\frac{1}{10}$ of solid density are created. The collision time depends mainly on the cavity size. In our simulation of a hohlraum of 1 mm (2 mm) diameter and an average laser intensity of 10^{14} W/cm^2 (2×10^{13} W/cm^2) collisional reheating starts at 1 ns (2.5 ns). If the time of collisional reheating overlaps partially with the laser heating period, a considerable temperature rise is the consequence. The simulation of our 1-mm lossless cavity gives a radiation flux enhancement of a factor 1.6. Otherwise, if the plasma collision occurs after the laser pulse, a second peak in the history of the temperature is observed. These two cases could be verified experimentally.

A comparison was made of results from our triple cavity experiment with analytical model calculations which do not include collision effects. The results show an acceptable agreement for the 2-mm cavities where the collision occurs later in time so that it does not have any influence on the main x-ray peak. The second peak itself was observed in the satellite cavities whereas hole closure leads to a strong decay of the measured x-ray flux from the central cavity. In the 1-mm cavity case, the experimentally observed temperature was evidently higher than the calculated one due to the overlap of laser pulse and collisional reheating. So the simulations illustrate the role of the expanding plasma for the heating of small cavities to high temperatures.

ACKNOWLEDGMENTS

The authors would like to thank J. Meyer-ter-Vehn for suggesting the possibility of simulating the spherical cavities using the 1D hydrocode MULTI and also S. Witkowski for reading the manuscript and making useful suggestions. This work was supported in part by the Commission of the European Communities in the framework of the Association Euratom-Max-Planck-Institut für Plasmaphysik.

[1] G. D. Tsakiris, P. Herrmann, R. Pakula, R. Schmalz, R. Sigel, and S. Witkowski, Europhys. Lett. **2**, 213 (1986).

[2] P. Herrmann, R. Pakula, I. B. Földes, R. Sigel, G. D. Tsakiris, and S. Witkowski, Z. Naturforsch. A **41**, 767 (1986).

[3] T. Mochizuki, T. Yabe, H. Azechi, K. A. Tanaka, T. Boehly, N. Miyanaga, H. Nishimura, S. Ido, M. Yamanaka, K. Nishihara, T. Norimatsu, T. Jitsuno, M. Nakatsuka, K. Mima, S. Nakai, C. Yamanaka, R. Sigel, G. D. Tsakiris, K. Eidmann, P. Herrmann, R. Pakula, P. Sachsenmaier, S. Sakabe, and S. Witkowski, in Proceedings of the Eleventh International Conference on Plasma Physics and Controlled Nuclear Fusion Research held by the International Atomic Energy Agency, Kyoto, 1986 [Nucl. Fusion Suppl. **3**, 25 (1987)].

[4] S. Sakabe, R. Sigel, G. D. Tsakiris, I. B. Földes, and P. Herrmann, Phys. Rev. A **38**, 5756 (1988).

[5] G. D. Tsakiris and R. Sigel, Phys. Rev. A **38**, 5769 (1988).

[6] G. D. Tsakiris, J. Massen, R. Sigel, F. Lavarenne, R. Fedosejevs, J. Meyer ter Vehn, K. Eidmann, S. Witkowski, H. Nishimura, Y. Kato, H. Takabe, T. Endo, K. Kondo, H. Shiraga, S. Sakabe, T. Jitsuno, M. Takagi, C. Yamanaka, and S. Nakai, Phys. Rev. A **42**, 6188 (1990).

[7] R. Sigel, G. D. Tsakiris, F. Lavarenne, J. Massen, R. Fedosejevs, J. Meyer-ter-Vehn, M. Murakami, K. Eidmann, S. Witkowski, H. Nishimura, Y. Kato, H. Takabe, T. Endo, K. Kondo, H. Shiraga, S. Sakabe, T. Jitsuno, M. Takagi, C. Yamanaka, and S. Nakai, in Proceedings of the Thirteenth International Conference on Plasma Physics and Controlled Nuclear Fusion Research held by the International Atomic Energy Agency, Washington, DC, 1990 [Nucl. Fusion Suppl. **3**, 81 (1991)].

[8] H. Nishimura, Y. Kato, H. Takabe, T. Endo, K. Kondo, H. Shiraga, S. Sakabe, T. Jitsuno, M. Takagi, C. Yamanaka, S. Nakai, R. Sigel, G. D. Tsakiris, J. Massen, M. Murakami, F. Lavarenne, R. Fedosejevs, J. Meyer ter Vehn, K. Eidmann, and S. Witkowski, Phys. Rev. A **44**, 8323 (1991).

[9] E. Strom, J. Fusion Energy **7**, 131 (1988).

[10] Y. Kato, H. Shiraga, H. Nishimura, T. Endo, K. Kondo, M. Katayama, M. Nakai, S. Miyamoto, H. Takabe, K. Nishihara, M. Takagi, T. Norimatsu, T. Yamanaka, T. Jitsuno, M. Nakatsuka, S. Nakai, T. Kanabe, and C. Yamanaka, in Proceedings of the Thirteenth International Conference on Plasma Physics and Controlled Nuclear Fusion Research held by the International Atomic Energy Agency, Washington, DC, 1990 [Nucl. Fusion Suppl. **3**, 89 (1991)].

[11] J. D. Lindl, R. L. McCrory, and E. M. Campbel, Phys. Today **45**, (9), 32 (1992).

[12] R. Sigel, G. D. Tsakiris, F. Lavarenne, J. Massen, R. Fedosejevs, J. Meyer ter Vehn, M. Murakami, K. Eidmann, S. Witkowski, H. Nishimura, Y. Kato, H. Takabe, T. Endo, K. Kondo, H. Shiraga, S. Sakabe, T. Jitsuno, M. Takagi, C. Yamanaka, and S. Nakai, Phys. Rev. Lett. **65**, 587 (1990).

[13] R. Sigel, G. D. Tsakiris, F. Lavarenne, J. Massen, R. Fedosejevs, K. Eidmann, J. Meyer ter Vehn, M. Murakami, and S. Witkowski, H. Nishimura, Y. Kato, H. Takabe, T. Endo, K. Kondo, H. Shiraga, S. Sakabe, T. Jitsuno, M. Takagi, S. Nakai, and C. Yamanaka, Phys. Rev. A **45**, 3987 (1992).

[14] R. Sigel, in *Handbook of Plasma Physics, Vol. 3: Physics of Laser Plasma,* edited by A. M. Rubenchik and S. Witkowski (Elsevier Science, Amsterdam, 1991), p. 163.

[15] Ya. B. Zel'dovich and Yu. P. Raizer, *Physics of Shock Waves and High-Temperature Hydrodynamic Phenomena* (Academic, New York, 1966).

[16] R. Pakula and R. Sigel, Phys. Fluids **28**, 232 (1985); **29**, 1340E (1986).

[17] R. Sigel, in *Laser Plasma Interactions 4,* edited by M. Hooper (SUSSP, Edinburgh, 1989).

[18] S. M. Pollanine, R. L. Berer, and C. J. Keane, Phys. Fluids B **4**, 989 (1992).

[19] R. Ramis, R. Schmalz, and J. Meyer-ter-Vehn, Comput. Phys. Commun. **49**, 475 (1988).

[20] G. D. Tsakiris and K. Eidmann, J. Quant. Spectrosc. Radiat. Transfer **38**, 353 (1987).

[21] R. Sigel, R. Pakula, S. Sakabe, and G. D. Tsakiris, Phys. Rev. A **38**, 5779 (1988).

[22] G. D. Tsakiris, Phys. Fluids B **4**, 992 (1992).

[23] K. Eidmann, R. F. Schmalz, and R. Sigel, Phys. Fluids B **2**, 208 (1990).

[24] J. Massen, Ph.D. dissertation, Ludwig Maximilians Universität, München, 1991, Max-Planck Institut für Quantenoptik Report No. MPQ-166, Garching bei München, 1992 (unpublished).

[25] R. J. Harrach and M. Gee, Rev. Sci. Instrum. **59**, 1851 (1988).

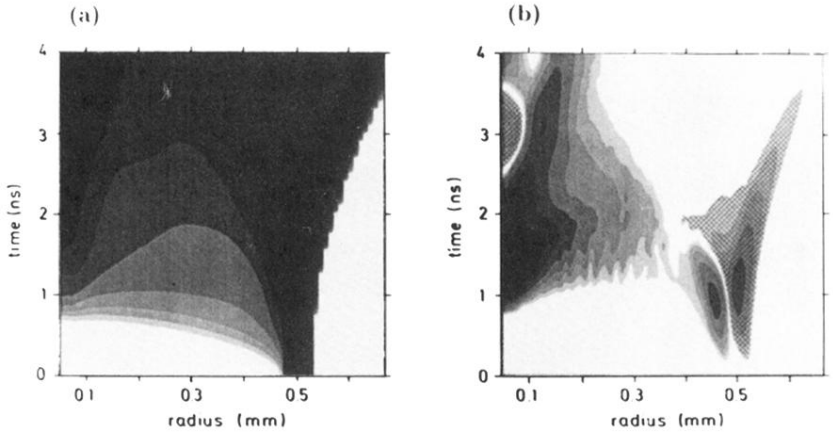

FIG. 4. Temporal and spatial evolution of (a) the density and (b) the divergence of the radiation flux in the interior of a lossless 1-mm cavity uniformly irradiated with $\sim 10^{14}$ W/cm^2 of $\lambda = 0.35$-μm (3ω)Nd-glass laser light having a pulse duration of $\tau_L = 0.9$ ns. In the contour plots, the values are normalized to the maximum, the steps are logarithmic, and comprise four decades in case (a) and two decades in case (b). Opposed to emission, absorption is characterized by the hatched area.

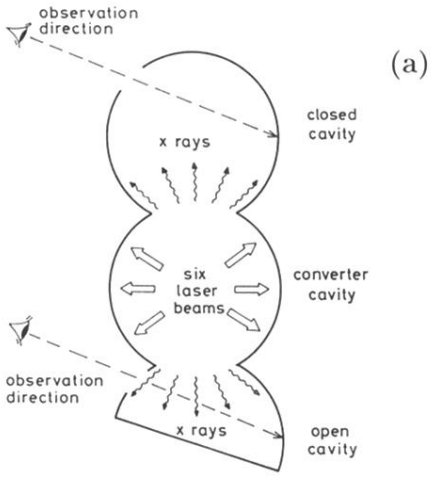

(a)

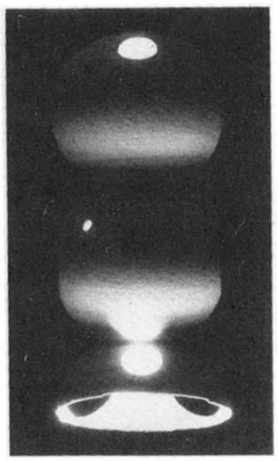

(b)

FIG. 5. (a) Schematic diagram showing the sequence of heating and the method of observation in the triple cavity targets. (b) Scanning electron microscope photograph of the real target.